

Extreme-Ultraviolet-Initiated High-Order Harmonic Generation: Driving Inner-Valence Electrons Using Below-Threshold-Energy Extreme-Ultraviolet Light

A. C. Brown^{*} and H. W. van der Hart

Centre for Theoretical Atomic, Molecular and Optical Physics, School of Mathematics and Physics,
Queen's University Belfast, Belfast BT7 1NN, United Kingdom

(Received 16 May 2016; revised manuscript received 7 July 2016; published 23 August 2016)

We propose a novel scheme for resolving the contribution of inner- and outer-valence electrons in extreme-ultraviolet (XUV)-initiated high-harmonic generation in neon. By probing the atom with a low-energy (below the $2s$ ionization threshold) ultrashort XUV pulse, the $2p$ electron is steered away from the core, while the $2s$ electron is enabled to describe recollision trajectories. By selectively suppressing the $2p$ recollision trajectories, we can resolve the contribution of the $2s$ electron to the high-harmonic spectrum. We apply the classical trajectory model to account for the contribution of the $2s$ electron, which allows for an intuitive understanding of the process.

DOI: 10.1103/PhysRevLett.117.093201

High-harmonic generation (HHG) is now a well-established tool both for the generation of high-energy and attosecond laser pulses [1,2] and as a measurement technique for atomic and molecular structure and ultrafast electron dynamics [3–5]. The well-known “three-step” model captures well the gross dynamics of the process: An electron is (i) ionized and then (ii) driven by a strong laser field before (iii) recolliding with its parent ion and releasing its energy in the form of a high-harmonic photon [6].

For some time now, researchers have been concerned with both the *optimization* of the process [7–9] and its *application* to measurement in so-called high-harmonic spectroscopy [3–5,10,11]. Both of these considerations raise the same conclusion: The initial step of the three-step model (tunnel ionization) limits both the conversion efficiency and the ability of HHG to probe general electron dynamics, restricted as it is to the emission of the outermost-valence electron. Hence, it has been proposed that, by subjecting the target to both the strong driving field and a short extreme-ultraviolet (XUV) pulse, the HHG process can be initiated by photoionization rather than tunnel ionization [8]. This has the advantage of being significantly more efficient and of opening the possibility of driving more deeply bound electrons.

Several theoretical studies have explored the efficiency question by utilizing simple model calculations to describe the three-step process [12,13]. A related scheme—wherein an XUV pulse excites a core electron to a valence hole during the valence electron’s transit—has also been studied [14–16]. More recently, an *XUV-initiated* HHG (XIHHG—i.e., the core, rather than the valence, electron is emitted in the initial step) scheme was used to elucidate core-hole dynamics in small molecules [17].

The attraction of studying core-hole dynamics is two-fold. First, the HHG cutoff is extended in proportion to the electron binding energy, and thus, by driving HHG with a

deeply bound electron, a substantial extension of the HHG plateau can be achieved. Not only does this allow the generation of ever-shorter, attosecond pulses, an extended cutoff also allows a greater scope for the analysis of the spectrum. Second, high-energy photoionization favors ionization of core rather than valence electrons, whereas the outer electrons are more susceptible to tunnel ionization and photoionization by lower-energy XUV light. Thus, to a reasonable approximation, only the core electron responds to the XUV photon, and the response of the outer electrons can be neglected.

However, one can envisage dynamics involving the correlated motion of inner- and outer-valence electrons which may be probed with XIHHG. For instance, the window resonances in the photoionization spectrum of argon are due to the interference of $3s$ and $3p$ electrons. We have previously shown that these interferences also impact on low-energy harmonic generation in short-wavelength (390 nm) fields [18]. To investigate their role in *high-harmonic* generation, driving wavelengths in the near- to mid-IR range should be employed, but at such low photon energies the response of the inner-valence electron is negligible. Thus, a combination of XUV and IR light might be used to probe such interference dynamics.

There are only a handful of computational methods capable of describing the multielectron dynamics necessary for a thorough exploration of HHG with inner-valence electrons [19,20]. Among them, the *R* matrix with time-dependence (RMT) technique has demonstrated significant promise for the description of ultrafast processes in general multielectron systems [21]. RMT has been applied variously to HHG in the computationally challenging near-IR wavelength regime [22], electron rescattering in negative ions [23], IR-assisted ultrafast ionization of positive ions [24], and attosecond transient absorption spectroscopy of doubly and core-excited states [25].

In the present Letter, we explore the XHHG process in neon and assess the contribution of the inner-valence electron to the resulting spectra. In contrast with previous studies, which promote the inner-valence electron during the transit of the outer-valence electron [14–16], we drive the inner-valence electron on a three-step-like trajectory by employing XUV pulse energies *below* the 2s ionization threshold. Additionally, we consider how the timing of the ultrashort XUV pulse can be used to selectively enhance the contribution of the 2s electron, an extension of the method previously explored by Schafer *et al.* [26].

The RMT method is an *ab initio* technique for solving the time-dependent Schrödinger equation for general, multi-electron atoms or ions in strong laser fields. We employ the well-known *R*-matrix paradigm, whereby the interaction space is split into two regions: an inner region—close to the nucleus, wherein full account is taken of all multielectron interactions—and an outer region—where a single, ionized electron moves under the influence of the laser field and the long-range potential of the core. Several implementations of the time-dependent *R*-matrix theory exist [27–30], but RMT offers the most robust and general numerical approach for tackling processes in strong fields. This is achieved through representing the wave function with a *B*-spline-based, *R*-matrix basis in the inner region and with a highly efficient grid-based approach in the outer region [21].

The neon target used for this study is discussed in detail elsewhere [31]. Briefly, the neon atom is described in a close coupling with pseudostates scheme as a Ne^+ ion plus an electron. The descriptions include all $2s^2 2p^5 e\ell$ and $2s 2p^6 e\ell$ channels up to $L_{\max} = 139$. The inner (outer) region boundary is 32 a.u. (2000 a.u.) (results are converged with respect to these boundaries). The set of continuum orbitals contains 70 *B* splines for each angular momentum of the continuum electron.

The primary laser pulse used is a three-cycle (18 fs), 1.8 μm pulse with an intensity of $1.2 \times 10^{14} \text{ W cm}^{-2}$. The XUV intensity is 10% of the IR intensity. Both the IR and XUV pulses have a \sin^2 ramp on-off profile. Unless otherwise stated, the delay between IR and XUV pulses is chosen to be 2.75 fs such that the XUV peak arrives one half-cycle before the IR peak. According to the classical three-step model, electrons “born” into the field at this time describe the optimal trajectories for HHG.

Calculations performed for various XUV intensities (1% and 0.1% of the IR intensity) show that the overall yield scales linearly with the XUV intensity. Calculations performed with 800 nm IR pulses instead of 1.8 μm show that the mechanisms discussed below also apply at the lower wavelength. We here display only the results for the 1.8 μm IR and 10% intensity XUV, as they support longer plateaus and a clearer observation of the key features. The probability to tunnel ionize from the 2p shell in the IR field is 0.00003% and to photoionize with the 45 eV XUV from the 2p or 2s is 0.3% and 0.002%, respectively.

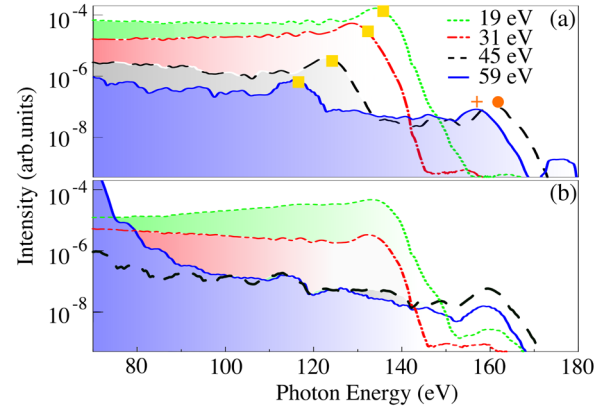


FIG. 1. The smoothed harmonic yield from Ne driven by an 18 fs, 1.8 μm , $1.2 \times 10^{14} \text{ W cm}^{-2}$ pulse, in combination with a (a) 1 fs and (b) 250 as XUV pulse of energy 19 (black dotted line), 31 (red dot-dashed line), 45 (green dashed line), and 59 eV (blue solid line). The cutoff of the 2p harmonics as predicted by the model (see the text) are marked by yellow squares. The predicted 2s cutoff is marked for the 45 (circle) and 59 eV (plus) XUV pulses.

We perform calculations for XUV-photon energies ranging from beneath the 2p binding energy ($E_{2p} = 21.6 \text{ eV}$) to above the 2s binding energy ($E_{2s} = 48.5 \text{ eV}$) and use two XUV pulse durations: 1 fs (“long”) and 250 as (“short”). Figure 1 shows the harmonic spectra for four XUV-photon energies—19, 31, 45, and 59 eV (corresponding to particular odd harmonics of the 1.8 μm pulse) in both the long- and short-pulse configurations.

At a photon energy of 19 eV (45 eV), the XUV pulse is not sufficiently energetic to ionize the 2p (2s) electron directly. However, the HHG yield is still increased by several orders of magnitude over the IR-only spectrum (not shown). We attribute this to a two-photon (IR + XUV) ionization process. These XUV-photon energies are resonant with a number of Rydberg states converging onto the 2p and 2s ionization thresholds, and thus photoexcitation to a (superposition of several) Rydberg state(s) is followed by field ionization. This two-stage process allows the electron to be born into the field with approximately zero energy, which is crucial for optimizing the three-step recollision process.

For XUV-photon energies of 45 and 59 eV, Fig. 1 shows an extension of the plateau, the cutoff of which is dependent on the XUV-photon energy. In the long-pulse case, there appears a double plateau structure, and the cutoff energy of the first plateau (marked by yellow squares) decreases with increasing photon energy.

To understand the extension of the cutoff, we consider the empirical formula for the cutoff energy [32]:

$$E_{\text{cutoff},2p} \approx 3.2U_p + I_p = 137 \text{ eV},$$

where U_p is the ponderomotive energy and I_p the ionization potential: i.e., the binding energy of the 2p electron, 21.6 eV. If instead we use the binding energy of the 2s electron, then we predict a cutoff of

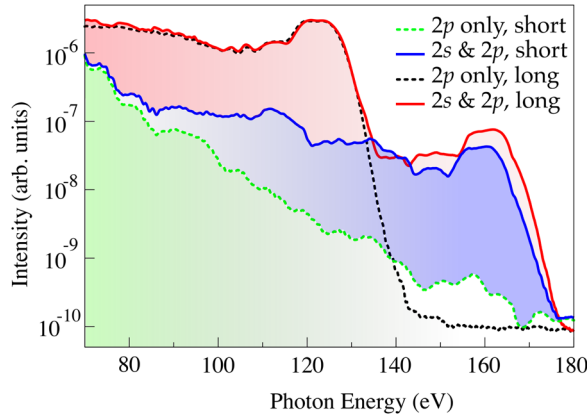


FIG. 2. The smoothed cutoff harmonics from Ne driven by an 18 fs, 1.8 μm , $1.2 \times 10^{14} \text{ W cm}^{-2}$ pulse, in combination with a 250 as (lower two lines) and 1 fs (upper two lines), 45 eV XUV pulse timed to coincide with the penultimate maximum of the IR field. Calculations include the action of both the 2s and 2p electrons (solid lines) or neglecting the action of the 2s (dotted lines).

$$E_{\text{cutoff},2s} \approx 3.2U_p + E_{2s} = 160 \text{ eV},$$

in line with the 45 eV XUV spectrum in Fig. 1.

In order to isolate the contribution of the 2s electron, two calculations are performed with an XUV-photon energy of 45 eV: one comprising both the $2s^22p^5$ and $2s2p^6$ Ne^+ thresholds and one with only the $2s^22p^5$. Removing the $2s2p^6$ threshold effectively neglects ionization of the 2s electron in the calculation. A similar approach was used to elucidate the contribution of the 3s and 3p electrons to low-energy harmonic generation in Ar [18].

Figure 2 shows the high-energy harmonics from Ne as generated with these two atomic structure configurations, for both the long and short XUV pulses. There is a clear difference between the spectra from the 2p-only and 2s – 2p calculations: The 2s – 2p yield shows a recognizable plateau extending to a cutoff at 160 eV which is not present in the 2p-only calculations for either long or short pulses. This confirms that the highest-energy harmonics are generated by the action of the 2s electron.

In the long pulse, there is no difference between the 2p-only and 2s – 2p spectra up to an initial cutoff at 125 eV. For the short pulse, the overall harmonic yield is largely suppressed, but the integrated yield above 100 eV is increased by an order of magnitude by the inclusion of the 2s electron. This is surprising, as the ionization probability for a 2s electron is around 1% of that of a 2p electron. Furthermore, the cutoff ascribed to the 2p electron—125 eV—does not agree with the classically predicted cutoff energy of 137 eV.

To elucidate these differences, we perform classical trajectory simulations: For each “birth time,” we can calculate the electron’s velocity and position by integrating

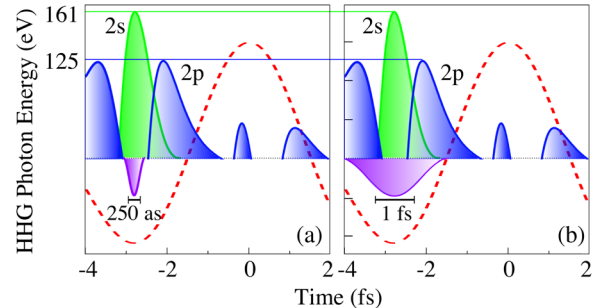


FIG. 3. The maximum emitted harmonic photon energies that would result from electrons being released at the times shown along the horizontal axis for both 2p (blue) and 2s (green) electrons from Ne in an 18 fs, 1.8 μm , $1.2 \times 10^{14} \text{ W cm}^{-2}$ pulse (red dashed line). Trajectories are initiated by a (a) 250 as and (b) 1 fs, 45 eV XUV pulse. Trajectories of 2s and 2p which lead to recollision are localized in time and therefore can be resolved in the short-pulse case (a). For a long XUV pulse (b), both electrons contribute.

over the acceleration in the IR field. Those trajectories which pass again through the origin describe recolliding electrons from which the recollision energy—and hence the energy of the HHG radiation—can be determined. Importantly, in general, a photoionized electron will be born into the field with nonzero velocity, while in the traditional three-step model the initial velocity of the tunnel-ionized electron is assumed to be zero [26]. This initial velocity is calculated directly from the excess energy absorbed by the electron, i.e., the difference between the XUV-photon energy and the ionization potential. We note that this velocity may be in any direction relative to the linearly polarized IR field. Thus, a 2p electron will gain an excess energy of 23.4 eV (45–21.6 eV), while a 2s electron is born with zero initial velocity (in practice, there will be a spread of initial energies due to the bandwidth of the XUV pulse, but we assume just one initial velocity for the purposes of the model).

Figure 3 shows the HHG photon energy for 2s and 2p electron recollision trajectories originating at different times in the IR pulse. The excess energy gained negates the recollision of 2p electrons born at the penultimate peak of the IR but allows those born earlier or later in the IR cycle to recollide. By contrast, the choice of an XUV-photon energy below the 2s ionization threshold ensures that the 2s electron is born with zero velocity. Thus, its recollision trajectories correspond to birth times around the penultimate peak of the IR field. As tunnel ionization due only to the IR field is negligible, we assume that only trajectories born during the XUV pulse contribute substantially to the HHG spectrum and—in the short-pulse case—this means only 2s electrons will contribute. This is despite the relatively low probability of ionizing a 2s electron versus a 2p electron.

By contrast, the long pulse does not resolve the contribution of the 2s and 2p electrons. Thus, both

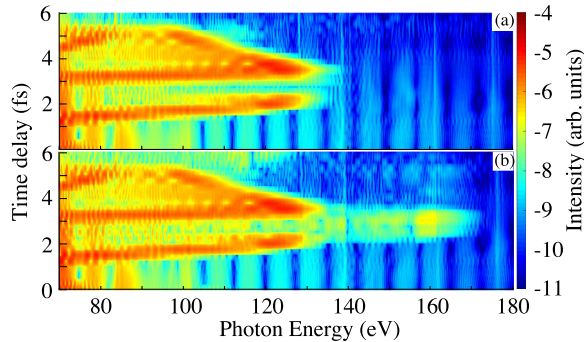


FIG. 4. The XIHHG spectrum for Ne as a function of the time delay between the XUV and IR pulse peaks for RMT calculations both (a) neglecting and (b) including the action of a $2s$ electron.

contributions are present. However, because the ionization probability for a $2p$ electron is 2 orders of magnitude larger than for a $2s$, the HHG yield up to the first cutoff is dominated by $2p$ electrons, and we elucidate the $2s$ contribution only above this energy. The initial velocity of the $2p$ electrons in the field modifies their trajectory from the tunnel-ionization case, reducing the maximum energy of the recolliding electron and hence the initial $2p$ cutoff of the HHG spectrum. The maximum energy calculated for the $2p$ electron is 125 eV, in line with the $2p$ cutoff observed in the spectra (Fig. 2).

In order to confirm the intuition of this simple model, we perform calculations for the XUV-photon energies shown in Fig. 1. The yellow squares shown are the predicted cutoff energies for the $2p$ trajectories as calculated by the model, while the orange circle and cross are those calculated for the $2s$ electron. They are seen to be in good agreement with the RMT results.

To confirm the two-stage ionization mechanism, we refer to Fig. 4, which shows the time-delay scans for two simulations for the 250 as, 45 eV XUV pulse for calculations including or neglecting the action of the $2s$ electron. The time window in which the $2p$ recollision is suppressed is clearly seen between 2.5 and 3.5 fs. This corresponds to a drop in the overall yield but an extension of the cutoff energy with the contribution of the $2s$ electron. The cutoff energy is in line with the prediction of the model calculations shown in Fig. 3. In particular, we observe an enhancement at the $2p$ cutoff for time delays around 2 and 4 fs which match the predictions of the model (the cutoff energy observed is higher than in the model calculations but within the bandwidth of the XUV pulse, which is not accounted for in the model).

Importantly, the extension of the cutoff due to the $2s$ electron is observed for time delays between 2.25 and 3.5 fs, corresponding to the XUV pulse arriving at, or just before, the IR peak. This confirms the proposed two-stage ionization mechanism, wherein the $2s$ electron is promoted into a $2s2p^5n\ell$ Rydberg state before being field ionized at the IR peak. This mechanism warrants further

investigation, as a scheme may be devised to probe sensitively the lifetimes of excited Rydberg states.

Because the binding energy of inner-valence electrons is not well separated from the ionization potential of the valence shell, XIHHG of inner-valence electrons will not provide substantial gains in cutoff energy. This could be accomplished more easily with the use of higher-intensity IR pulses or indeed with XIHHG of more deeply bound electrons. However, the scheme still represents more promise than may previously have been thought. Because of the relatively small probability of ionizing an inner-valence electron—even with an XUV pulse tuned to the correct binding energy—the outer-valence electron should dominate the HHG process, and indeed, for long XUV pulses we observe that the yield from neon is dominated by the $2p$ electron contribution up to the $2p$ cutoff. However, we have shown that with short pulses, whose energy is below the $2s$ ionization energy, it is possible to selectively suppress the contribution of $2p$ electrons and elucidate the contribution of the $2s$ electron, even if this results in a much lower overall yield.

Thus, for attosecond duration XUV pulses delayed appropriately with respect to the IR field, it should be possible to perform HHG spectroscopy of inner-valence electrons. If appropriate pulse profiles or as-pulse trains can be devised, both inner- and outer-valence electrons may contribute on a similar magnitude. This would then facilitate HHG spectroscopy of interference dynamics as previously explored for low-energy harmonics [18].

The data used in this paper may be accessed at Ref. [33].

H. W. H. acknowledges financial support from the United Kingdom EPSRC under Grant No. EP/G055416/1 and the EU Initial Training Network CORINF. This work used the ARCHER United Kingdom National Supercomputing Service.

* andrew.brown@qub.ac.uk

- [1] K. Zhao, Q. Zhang, M. Chini, Y. Wu, X. Wang, and Z. Chang, *Opt. Lett.* **37**, 3891 (2012).
- [2] P. M. Paul *et al.*, *Science* **292**, 1689 (2001).
- [3] A. D. Shiner, B. E. Schmidt, C. Trallero-Herrero, H. J. Wörner, S. Patchkovskii, P. B. Corkum, J.-C. Kieffer, F. Légaré, and D. M. Villeneuve, *Nat. Phys.* **7**, 464 (2011).
- [4] O. Smirnova, Y. Mairesse, S. Patchkovskii, N. Dudovich, D. Villeneuve, P. Corkum, and M. Yu. Ivanov, *Nature (London)* **460**, 972 (2009).
- [5] J. Itatani, J. Levesque, D. Zeidler, H. Niikura, H. Pépin, J. C. Kieffer, P. B. Corkum, and D. M. Villeneuve, *Nature (London)* **432**, 867 (2004).
- [6] P. B. Corkum, *Phys. Rev. Lett.* **71**, 1994 (1993).
- [7] E. J. Takahashi, T. Kanai, K. L. Ishikawa, Y. Nabekawa, and K. Midorikawa, *Phys. Rev. Lett.* **99**, 053904 (2007).
- [8] M. B. Gaarde, K. J. Schafer, A. Heinrich, J. Biegert, and U. Keller, *Phys. Rev. A* **72**, 013411 (2005).

- [9] F. Brizuela, C. M. Heyl, P. Rudawski, D. Kroon, L. Rading, J. M. Dahlström, J. Mauritsson, P. Johnsson, C. L. Arnold, and A. L'Huillier, *Sci. Rep.* **3**, 1410 (2013).
- [10] O. Smirnova and O. Gessner, *Chem. Phys.* **414**, 1 (2013).
- [11] P. M. Kraus and H. J. Wörner, *Chem. Phys.* **414**, 32 (2013).
- [12] J. Biegert, A. Heinrich, C. P. Hauri, W. Kornelis, P. Schlup, M. P. Anscombe, M. B. Gaarde, K. J. Schafer, and U. Keller, *J. Mod. Opt.* **53**, 87 (2006).
- [13] G. Gademann, F. Kelkensberg, W. K. Siu, P. Johnsson, M. B. Gaarde, K. J. Schafer, and M. J. J. Vrakking, *New J. Phys.* **13**, 033002 (2011).
- [14] C. Butth, *Eur. Phys. J. D* **69**, 234 (2015).
- [15] C. Butth, M. C. Kohler, J. Ullrich, and C. H. Keitel, *Opt. Lett.* **36**, 3530 (2011).
- [16] M. Tudorovskaya and M. Lein, *J. Mod. Opt.* **61**, 845 (2014).
- [17] J. Leeuwenburgh, B. Cooper, V. Averbukh, J. P. Marangos, and M. Ivanov, *Phys. Rev. Lett.* **111**, 123002 (2013).
- [18] A. C. Brown, S. Hutchinson, M. A. Lysaght, and H. W. van der Hart, *Phys. Rev. Lett.* **108**, 063006 (2012).
- [19] L. Greenman, P. J. Ho, S. Pabst, E. Kamarchik, D. A. Mazzotti, and R. Santra, *Phys. Rev. A* **82**, 023406 (2010).
- [20] H. Miyagi and L. B. Madsen, *Phys. Rev. A* **87**, 062511 (2013).
- [21] L. R. Moore, M. A. Lysaght, L. A. A. Nikolopoulos, J. S. Parker, H. W. van der Hart, and K. T. Taylor, *J. Mod. Opt.* **58**, 1132 (2011).
- [22] O. Hassouneh, A. C. Brown, and H. W. van der Hart, *Phys. Rev. A* **90**, 043418 (2014).
- [23] O. Hassouneh, S. Law, S. F. C. Shearer, A. C. Brown, and H. W. van der Hart, *Phys. Rev. A* **91**, 031404 (2015).
- [24] H. W. van der Hart and R. Morgan, *Phys. Rev. A* **90**, 013424 (2014).
- [25] T. Ding *et al.*, *Opt. Lett.* **41**, 709 (2016).
- [26] K. J. Schafer, M. B. Gaarde, A. Heinrich, J. Biegert, and U. Keller, *Phys. Rev. Lett.* **92**, 023003 (2004).
- [27] X. Guan, O. Zatsarinny, K. Bartschat, B. I. Schneider, J. Feist, and C. J. Noble, *Phys. Rev. A* **76**, 053411 (2007).
- [28] M. A. Lysaght, H. W. van der Hart, and P. G. Burke, *Phys. Rev. A* **79**, 053411 (2009).
- [29] L. Torlina and O. Smirnova, *Phys. Rev. A* **86**, 043408 (2012).
- [30] L. Torlina, M. Ivanov, Z. B. Walters, and O. Smirnova, *Phys. Rev. A* **86**, 043409 (2012).
- [31] P. G. Burke and K. T. Taylor, *J. Phys. B* **8**, 2620 (1975).
- [32] J. L. Krause, K. J. Schafer, and K. C. Kulander, *Phys. Rev. Lett.* **68**, 3535 (1992).
- [33] <http://pure.qub.ac.uk/portal/en/datasets/search.html>.